(This is a sample cover image for this issue. The actual cover is not yet available at this time.)

Journal of Luminescence 132 (2012) 1106–1111

Contents lists available at SciVerse ScienceDirect

Journal of Luminescence

journal homepage: www.elsevier.com/locate/jlumin

X-ray excited optical luminescence of Ce-doped $BaAl_2O_4$

Marcos V. dos S. Rezende [a,*], Paulo J.R. Montes [b], Mário E.G. Valerio [a]

[a] Physics Department, Federal University of Sergipe, Campus Universitário, 491000-000 São Cristovão-SE, Brazil
[b] Federal Institute of Sergipe-IFS, 49400-000 Largato-SE, Brazil

ARTICLE INFO

Article history:
Received 12 April 2011
Received in revised form
1 December 2011
Accepted 21 December 2011
Available online 31 December 2011

Keywords:
X-ray excited optical luminescence
Barium aluminates
Cerium
Scintillation

ABSTRACT

The luminescence properties of Ce^{3+} in $BaAl_2O_4$ are reported. The results of simultaneous measurements of XEOL and XAS in the X-ray energy range that includes the Ba $L_{II,III}$-edges and Ce L_{III} edge are shown. The XEOL yield increases as the energy of the photons increases. The radioluminescence spectra, taken from 200 to 1100 nm, showed broad emission bands corresponding to $5d^1 \rightarrow {}^2F_{5/2}$, ${}^2F_{7/2}$ transitions of Ce^{3+} when incorporated into two nonequivalent Ba sites. The lifetime of the light emission was also measured using the single bunch operation mode at the Brazilian National Synchrotron Laboratory (LNLS), and $BaAl_2O_4:Ce^{3+}$ showed single exponential decay time component of about 44.3 ns.

1. Introduction

Scintillating materials are widely used to detect γ-rays, X-rays and high energy particles. Scintillation is an example of radioluminescence where the absorption of the energy of the radiation or particles is transformed into UV–visible light. This property can be used for a number of applications in medical image, geophysical exploration and numerous other scientific and industrial applications [1].

The Ce^{3+} ion is one of the activators commonly used for the scintillator devices. It has been studied in a number of host lattices. The Ce-doped materials are good candidates for fast scintillators due to their spin allowed $5d^1$–$4f^1$ transitions. Examples of Ce-doped materials scintillators are $LiCaAlF_6$:Ce [2], $LaCl_3$:Ce [3] and $LuAlO_3$:Ce and $YAlO_3$:Ce [4].

The Ce^{3+} doping into $BaAl_2O_4$ also shows several other interesting optical properties. $BaAl_2O_4:Ce^{3+}$ and $BaAl_2O_4:Ce^{3+}$, Dy^{3+} were reported by Jia and co-workers [5] as long lasting phosphorescence materials that can be observed by the naked eyes in darkness for as long as 10 h when excited by ultra-violet light. The photoluminescence in the $BaAl_2O_4:Mn^{2+}$, Ce^{3+} is also reported [6]. $BaAl_2O_4$ matrix was also doped with several other rare earth ions. For example, $BaAl_2O_4:Eu^{2+}$, Dy^{3+}[7] and $BaAl_2O_4:Eu^{2+}$, Nd^{3+}[8] also exhibit long lasting phosphorescence properties and films of $BaAl_2O_4:Tm^{3+}$, $BaAl_2O_4:Tb^{3+}$ and $BaAl_2O_4:Eu^{3+}$[9] were reported as having interesting luminescence properties.

In this work, the optical response of nanopowders of $BaAl_2O_4:Ce^{3+}$, prepared via new proteic sol–gel method were investigated. $BaAl_2O_4:Ce^{3+}$ was shown in to exhibit radioluminescent emission when excited with X-rays and that points out to a possible use in the scintillator devices. X-ray excited optical luminescence (XEOL) with selected photon energy around the Ba L_{III} and L_{II}-edges and Ce L_{III}-edge were studied. XEOL spectrum was collected using an optical spectrometer simultaneously with the usual X-ray absorption near edge structure (XANES) and extended X-ray absorption fine structure (EXAFS) spectrum. The XEOL life time was measured using the synchrotron radiation in the single-bunch mode.

2. Experimental

The proteic sol–gel route [10] was used to produce nanopowders of $BaAl_2O_4$ and $Ba_{0.97}Al_2O_4:Ce_{0.03}$. This technique uses the coconut water (*Cocos nucifera*) as the starting solvent of the metal salts. The samples were prepared by mixtures of $Ba(NO_3)_2$, $Al(NO_3)_3 \cdot 9H_2O$ and $CeCl_3 \cdot 6H_2O$ to coconut water (*C. nucifera*). This mixture was dried at 100 °C for 24 h, forming a xerogel. The xerogel was calcined at 1100 °C for 2 h in an open air atmosphere. This technique is applied successfully in the $SrAl_2O_4$ [11]. X-ray diffraction powder measurements, using CuKα radiation in a Rigaku Ultima+RINT 2000/PC diffractometer, were carried out to analyze the structure of the samples.

XANES, EXAFS and XEOL experiments were performed in the Brazilian Synchrotron Light Laboratory—LNLS source in Campinas, São Paulo, Brazil, around the Ba L_{III-II} edges and Ce L_{III} edge at the X-ray absorption fine structure (D08B-XAFS-2) beamline using the

* Corresponding author. Tel.: +55 79 9932 2462.
E-mail address: mvsrezende@gmail.com (M.V.S. Rezende).

0022-2313/$ - see front matter © 2011 Elsevier B.V. All rights reserved.
doi:10.1016/j.jlumin.2011.12.064

multi-bunch operation in the transmission mode. The X-ray excited optical luminescence (XEOL) was measured simultaneously with the XANES/EXAFS spectra using an Ocean Optics HR2000 spectrometer equipped with an optical fiber to detect the UV/visible fluorescence. The lifetime experiments were realized also at D08B-XAFS-2 beamlines using the single-bunch mode operation of the synchrotron, with pulse interval of 311 ns and pulse FWHM of about 100 ps. The light detection apparatus for the lifetime measurements was composed by a HAMATSU R924 photomultiplier, a high voltage power supply and a Tektronix TDS684B oscilloscope. The light pulse was collected in the PMT and the current pulse was injected in one of the oscilloscope channels, using the internal 50 Ω internal resistance load. The second channel of the oscilloscope was connected to the square wave trigger signal coming from the synchrotron storage ring, used to synchronize the light pulse with the electrons bunch in the ring. With this arrangement the time resolution was estimated to be around 10 ns. The upper limit for the XEOL lifetime is estimated to be around 200 ns due to the 4.8 MHz repetition rate of the single bunch in the storage ring.

3. Results and discussion

The XRD patterns of the as prepared nanopowders (pure and doped) after heat treatment are shown in Fig. 1. The XRD patterns of the compounds are compared with the Huang et al. [12] standard diffraction pattern. It can be observed that only the $BaAl_2O_4$ $P6_3$ hexagonal phase exists in both the samples with a good degree of crystallinity, using temperature and time lower than that normally used for the conventional solid-state routes. Jia et al. [5], as an example, reported the need for two steps of thermal treatment to obtain their samples, the first one at 900 °C for 2 h and the second one at 1350 °C for 25 h. Suriyamurth et al. [6] using the conventional solid-state route, reported the need for two stages to obtain the right crystalline phase, the first one at 1000 °C for 5 h and the second at 1300 °C for 5 h. Thus, the results obtained in the present work attest the advantage of the proteic sol–gel methodology as compared to the other routes.

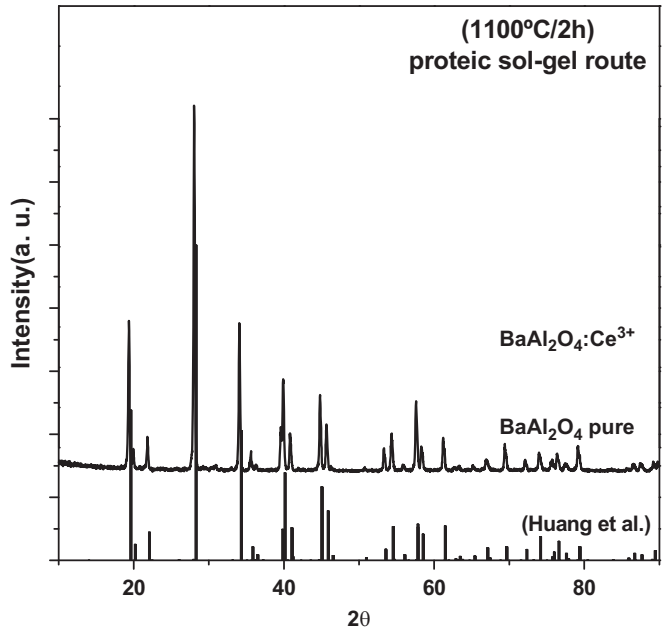

Fig. 1. X-ray powder diffraction patterns of pure and doped $BaAl_2O_4$.

The XANES spectrum of $BaAl_2O_4:Ce^{3+}$ excited in the range from 5200 to 5800 eV, covering the Ba L_{II} and L_{III} edges and Ce L_{III} edge, is shown in Fig. 2. The XANES spectrum was measured in the transmission mode. As expected, the spectrum is dominated by two intense lines at about 5249 eV and 5626 eV, associated to the Ba L_{III}-edge and L_{II}-edge, respectively. The Ce L_{III}-edge is observed as a bump at about 5735 eV due the superposition with the EXAFS region of Ba L_{III}-edge.

The XEOL spectrum is obtained simultaneously to the XAS spectrum. The XEOL spectrum is done in the following way: (i) for each incident X-ray photon energy a full UV to visible optical radioluminescence (RL) spectra is recorded, (ii) the area under the RL spectra is calculated and (iii) the area is plotted as a function of the incident X-rays photon energies (dotted curve in Fig. 2). The XEOL spectra presented roughly the same spectral features as the XANES/EXAFS spectra of the Ba L absorption edges. The main difference is that the pre- and post-edge of the XEOL curve presented an increasing trend as the energy of the photons increased while in the normal absorption curve the pre- and post-edges showed a decreasing behavior as the energy of the incident photon increased. This indicates that more intense radioluminescence is found for higher values of the energies of the excitation photons, although the total absorption of the sample decreased. This behavior of the XEOL is due to a series of processes that occur simultaneously during irradiation. First, Ba and Ce ions absorb the incident X-ray and decays mainly via two competing processes: the X-ray fluorescence emission and the Auger process. The main fluorescence emission are $L_{\alpha 1}$ (4466.5 eV) and $L_{\beta 2}$ (5154.4 eV), when excited at Ba L_{III}-edge (5247.0 eV), and $L_{\beta 1}$ (4828.3 eV) and $L_{\gamma 1}$ (5531.4 eV), when excited at Ba L_{II}-edge (5624.0 eV). The fluorescence emission of Ba ions are not efficiently absorbed by other ions of the crystalline matrix since they are much greater than the energies required to excite the K edges of Al or O, at 1559.0 eV and 543.1 eV, respectively. The X-ray fluorescence lines of Ba are ~1 keV lower than the L Ce absorption edges, and much higher than any of the Ce M absorption edges. Therefore, in this process there is very few direct energy transfer from the Ba X-ray fluorescence line that would cause ionization of the Ce ions decreasing the luminescence due to the Ce^{3+} ions. In the case of Ba the Auger process is quite important. About 80% [13] of the excited Ba ions, decays via the Auger processes that involves M electrons filling the hole in the L edge and the energy released is used to excite another M electron. So, instead of one electron–hole pair, the Auger process generates atleast 2 electron–hole pairs in the matrix, increasing the number of electron–hole pairs in the conducting—valence

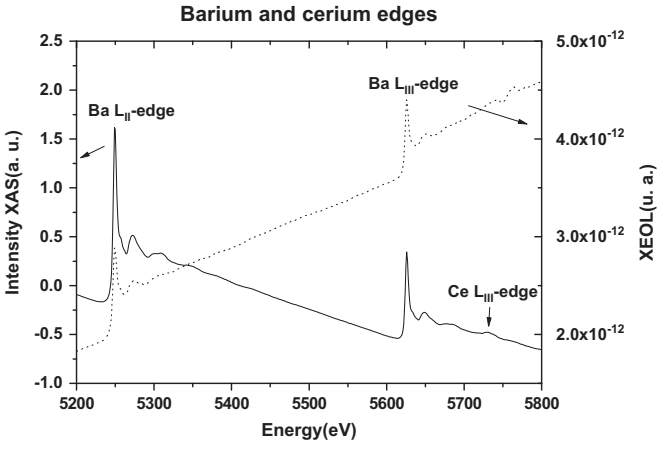

Fig. 2. XAS and XEOL curves of $BaAl_2O_4:Ce^{3+}$ excited in the region of L_{II} and L_{III} Ba edges and L_{III} Ce edge.

bands of the material. As the energy of the X-ray increases and becomes higher than the L_{III} or L_{II} absorption edges of Ba, the primary excited electrons will have a net kinetic energy that also increases. These "free" electrons in the conduction band can have enough kinetic energy to scatter other electrons and the electron–electron inelastic scattering probability increased, thus increasing the number of secondary electron–hole pairs. The recombination of the charge carrier pairs can now directly excite the Ce ions that decays from $5d^1$ excited state to the $4f^1$ ground states, thus increasing the XEOL yield.

The X-ray absorption at Ce L_{III}-edge (5723.0 eV) generates two main fluorescence lines at $L_{\alpha 1}$ (4839.2 eV) and $L_{\beta 2}$ (5614.0 eV) that can directly excite the Ba L_{II} and L_{III} edges. As a consequence, all the processes described above are trigged and the XEOL emission is also enhanced. A schematic representation of the processes involved in the XEOL emission of the $BaAl_2O_4$:Ce samples can be observed in Fig. 3.

In the XEOL curve, the jumps in the energy values corresponding to the Ba $L_{III,II}$-edges is observed but the one related to the Ce L_{III}-edge is not evident. This shows that the luminescence properties are connected mainly to the X-ray absorption by Ba ions in the matrix and weakly connected to the absorption by the dopant ions. The contribution due to the Ce absorption is indirect, transferring the absorbed energy to the Ba matrix and receiving it back when the electron–hole pairs recombine, as explained previously.

The radioluminescence spectra excited at the Ce L_{III}-edge were measured for the pure and doped sample at room temperature and they are shown in Fig. 4. As seen in Fig. 4, there are no observed bands or emission line for the pure samples. For the doped sample, three main bands are observed, two strong and broad emissions around 380 nm and 515 nm and one weak and broad emission around 725 nm.

The weak emission cannot be attributed to the splitting due to the $5d^1 \rightarrow {}^2F_{5/2}$ and $5d^1 \rightarrow {}^2F_{7/2}$ levels. The difference between the 715 and 515 nm bands is around 5400 cm^{-1} and that is a much bigger value than the expected one for the spin–orbital splitting ${}^2F_{5/2,7/2}$ of Ce^{3+} ions, typically smaller than 2200 cm^{-1}. This weak emission also cannot be caused by the transition of an electron from the conduction band to the $(5d^1)$ excited states of Ce^{3+}. If that occurred, Ce^{2+} species in the excited state would be formed and that is not a stable valence for Ce. One possible explanation is that this emission band is generated by the transitions among the $5d^1$ levels. Since the five 5d levels are exposed to the crystalline

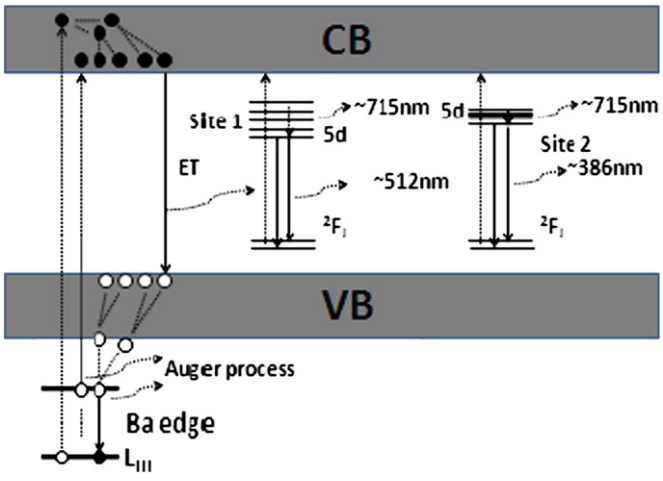

Fig. 3. XEOL mechanism in the $BaAl_2O_4$:Ce.

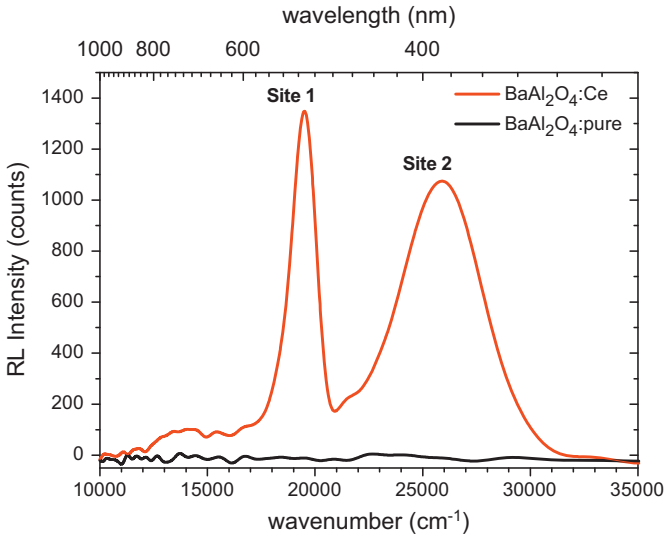

Fig. 4. Spectrum XEOL excited at Ce L_{III}-edge.

matrix, they are very much influenced by the crystalline field [14]. The symmetry for both Ce sites in the matrix is very distorted and that will cause the 5d levels to split. Krupa and Queffeleq [15] measured the absorption spectra of $LiYF_4$ doped with rare earth trivalent ions and they showed that the total splitting of the five $5d^1$ levels of Ce^{3+} in $LiYF_4$ is about 2.3 eV corresponding to ~18,860 cm^{-1}. The Ce site symmetry in $LiYF_4$ is S_4 and the Ce substitute at the Y site requires no charge compensation.

Shi et al. [16] showed that the 10 Dq crystal field parameter can be related to the difference in the barycenter of the two groups of $5d^1$ levels, t_{2g} and e_g, of Ce^{3+} in different fluoride matrixes. They collected different halide systems doped with Ce^{3+} where 10 Dq ranges from 6000 up to almost 14,000 cm^{-1}. They also found that 10 Dq follows a simple equation that involves four parameters:

$$F_C = \frac{E_h Q f_i}{N} \quad (1)$$

where E_h is the homopolar part of an average energy gap that has a simple relation with the bond length of the Ce^{3+} and the ligand, N is the coordination number of central ion, f_i is the bond iconicity between the central ion to nearest neighbors and Q is the charge of the neighboring anion. All values defining the F_c parameters can be evaluated for the $BaAl_2O_4$ case for the 2 possible Ce^{3+} centers and the average value for 10 Dq predicted by the Shi et al. formula is around 11,000 cm^{-1}. Considering that the Ce symmetry in $BaAl_2O_4$ is far from the octahedral symmetry and is much distorted, one would expect that all $5d^1$ levels will be split and it could be possible to observe internal transitions due to these $5d^1$ levels in a broad energy range.

The broad 725 nm (13,793 cm^{-1}) emission band shown in Fig. 4 spreads from 909 nm (~11,000 cm^{-1}) to 571 nm (~17,500 cm^{-1}), and this is thus consistent with the $5d^1$ internal transitions. The fact that this band is much weaker than the other ones can also be understood in this scenario considering that the higher probability would be the transition from any $5d^1$ excited states to one of the $4f^1$ ground states rather than the internal $5d^1$ transitions.

The intense emissions at 380 and 515 nm, on the other hand, are caused by the transition from the $(5d^1)$ excited states to the spin–orbit split ${}^2F_{5/2,7/2}$ components of the Ce^{3+} $(4f^1)$ ground state. The $5d^1 \rightarrow {}^2F_{5/2}$, ${}^2F_{7/2}$ transitions of Ce^{3+} are dipole allowed and the $5d^1$ levels are sensitive to the crystal field, as discussed before.

The existence of 2 broad bands associated to the $5d^1 \rightarrow {}^2F_{5/2}$, $^2F_{7/2}$ transitions is an indication that at least 2 non-equivalent sites of Ce^{3+} exist in the sample.

When the Ce ion is incorporated into the $BaAl_2O_4$ matrix, two possibilities can be considered. The incorporation can occur at the Al or the Ba sites, where charge compensation is needed. Previous works from the atomistic simulation showed that Ce dopant in $BaAl_2O_4$ tends to be incorporated at the Ba site with compensation provided by oxygen interstitials [17] and that Ce ion can be sited into two non-equivalent Ba sites. The difference in the local symmetry for both the Ce sites is quite large, caused by the non-equivalent distortion of the lattice induced by Ce itself and by oxygen interstitials, energetically favorable charge compensating defect after relaxation. This difference can be observed in Fig. 5 where both Ce sites are schematically shown (site 1 and site 2) with the first neighbor oxygen ion positions obtained after relaxation of the lattice and energy minimization [17]. The crystal field splitting for the $5d^1$ and for the $4f^1$ levels will be quite different for these two Ce sites. The splitting of the ^2F ground state of Ce^{3+} into site 1 and site 2 can be confirmed using a hybrid computer modeling method, based on a combination of crystal field calculations, and energy minimization [18]. These calculations will be done and presented in future works.

The influence of the crystal field in the Ce energy levels can be also observed when the Ce is doping different host matrixes. In Mares et al.'s work [19] the emission spectra of various Ce-doped scintillating crystals are reported. They showed that, in the YAP:Ce, the $5d^1 \rightarrow {}^2F_{5/2}$, $^2F_{7/2}$ transitions occur between 310 and 420 nm and in the YAG:Ce and LuAG:Ce matrix the emissions are found between 490 and 630 nm. The results confirm that, depending on the site symmetry of the dopant, the region where the $5d^1 \rightarrow {}^2F_{5/2}$, $^2F_{7/2}$ emission bands are located can be different.

The emission spectrum of $BaAl_2O_4$:Ce^{3+} excited in the near or vacuum ultraviolet (UV–VUV) spectral region reported by Jia and co-workers [5] also exhibit two emission peaks at 402 nm and 450 nm, when their samples are excited at 335 and 357 nm, respectively. Both peaks were attributed by the authors to the presence of Ce^{3+} at two different lattice sites. The two emission bands are at different positions as compared to the ones shown in this work and there are two possible reasons for that difference. The first one is related to the way the Jia et al. measured the emission spectra. Their excitation spectrum is obtained fixing the emission wavelength and that may hinder any possible peak shift as the excitation moves to a lower wavelength (higher photon energies). In their paper it is not mentioned if they checked this. Also there is no indication on the wavelength resolution of the monochromators. Since the excitation wavelength is close to the emission and considering that the excitation intensity is always much higher than the emission one, any scattered light from the excitation source may also disturb the emission. In the present work, Ce^{3+} emission is obtained exciting with the X-ray photons three orders of magnitude higher than the energy of the emission photons. So no contamination in the emission spectra could be seen. The second reason for the difference in the position of the Ce^{3+} $5d^1 \rightarrow {}^2F_{5/2}$, $^2F_{7/2}$ transitions might also be related with the sample itself. Jia and co-workers produced their samples in a single step solid state reaction by mixing $BaCO_3$, Al_2O_3 and stoichiometric quantity of $Ce_2(CO_3)_3$ with the addition of B_2O_3 as flux. They do not show any XRD pattern showing that they really have Ce doped $BaAl_2O_3$ in the end, although it would be expected that atleast a certain amount of $BaAl_2O_4$ would be formed, after their heat treatment program. Three issues should be raised here. Did all the Al_2O_3 react with the $BaCO_3$ forming $BaAl_2O_3$? Did all the Ce^{3+} dissolve in the $BaAl_2O_4$ matrix? If part of the Ce^{3+} stayed in a spurious phase, that would produce emission bands in a different position. The last one is the presence of B_2O_3 that can induce extra defects in the matrix changing the local crystal field that, in turn, would shift the emission bands due to Ce^{3+}. All these, unfortunately, cannot be checked because there is no XRD measurement quoted in the paper nor in a previous work from the same authors.

Suriyamurthy and Panigrahi [6], on the other hand, using a somewhat similar route to produce their doped $BaAl_2O_4$ samples quoted that they measured the XRD powder pattern and they found no evidence of a secondary phase. But, they measured the emission spectra of Ce^{3+} doped $BaAl_2O_4$ exciting at 350 nm, obtaining a emission spectra centered at 415 nm. But, this excitation wavelength is not enough to excite the emission from the other Ce^{3+} center with emission at 350 nm, as pointed out in the present work. Suriyamurthy and Panigrahi quoted a excitation spectra measured from 200 to 400 nm but they also kept the emission wavelength fixed at 415 nm and did not check for any shift in the emission or if there is another emission band. It should also be noted that the results presented by Suriyamurthy and Panigrahi did not agree with the ones presented by Jia and co-workers and that may reflect the different experimental setup and/or sample quality.

The scintillation decay time of the $BaAl_2O_4$:Ce^{3+} samples were measured during the single-bunch mode at the Brazilian Synchrotron Light Laboratory (LNLS) using excitation energy around 5723.0 eV. The decay time curves of the $BaAl_2O_4$:Ce^{3+} measured at room temperature are shown in Fig. 6. The result shown in Fig. 6 represents an average of several thousands of sequential measurements. The comparison of the response of the

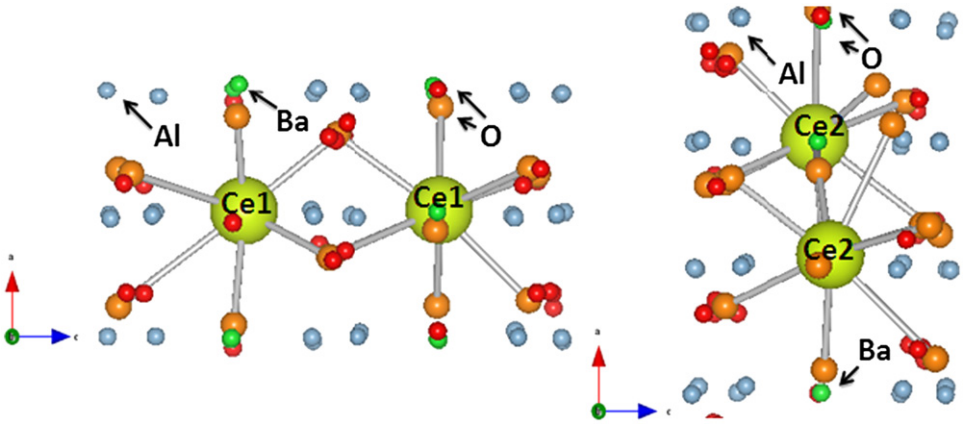

Fig. 5. Ce ions and the first neighbors after minimization of lattice.

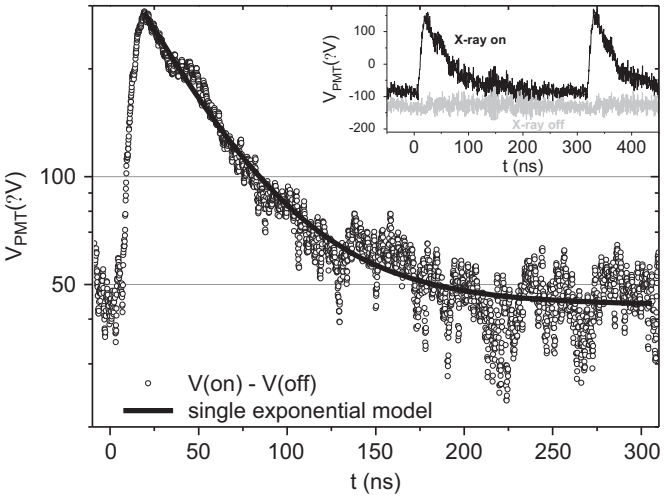

Fig. 6. Time decay of the XEOL excited at 5723 eV. Open circle represents the experimental values obtained subtracting the average PMT readings with no X-rays to the average readings obtained when the sample is exposed to the X-ray beam. The line is fitting to the single exponential decay model represented by Eq. (2). In the inset, two sequential light pulses are shown synchronous with the X-ray pulses. The gray curve represents the PMT signal obtained when the X-ray shutter is closed.

$BaAl_2O_4$:Ce^{3+} samples with and without pulsed X-ray excitation is shows in the inset of Fig. 6. Two sequential pulses are shown as recorded by the PMT coupled to the oscilloscope. The gray curve represents the background signal when the X-ray shutter is closed. The result of the net signal is shown as open circles, where the background PMT reading is subtracted from the PMT reading of the sample exposed to the X-rays pulses. The decay curves can be fitted to a single exponential decay model, according to the following equation:

$$I = I_0 \exp\left(-\frac{t}{\tau}\right) + I_{phosp} \quad (2)$$

where I represents the luminescence intensity at a time t after the X-ray pulse; I_0 is the emission intensity at $t=0$ ns, τ is the characteristic decay time of the process and I_{phosp} is the persistent emission of the sample, also known as phosphorescence. The fitting procedure (solid line in Fig. 6) provided a decay time constant of (44.3 ± 0.2) ns. This is a typical value of decay time luminescence process related to the Ce^{3+} ions since the $5d^1 \rightarrow {}^2F_{7/2,5/2}$ transitions are electric dipole allowed ones. The value obtained in this work agrees well to the typical Ce^{3+} decay time in several materials. The Ce^{3+} usually shows a fast luminescence with a decay time typically ranging from 15 to 100 ns. Such fast decay time were reported in YAP:Ce^{3+}(25–30 ns) [20], YAG:Ce (58 ns) [21], LuAG:Ce (50 ns) [21], $LaCl_3$:Ce (25 ns) [3], $LiBaF_3$:Ce (70 ns) [21], $LiYF_4$:Ce (65 ns) [22] and $LuAlO_3$:Ce (17.1–21.4 ns) [23], most of them are the bases for commercial scintillators. The decay curve represents the integral contribution of two Ce^{3+} ions. Although the two Ce^{3+} sites emit at different wavelengths, the excitation of both Ce^{3+} centers are done via the recombination of electrons and holes transferring the energy to the dopant, as discussed earlier. So the decay time of the luminescence will depend greatly on the overall traffic of charge carriers and one may speculate that the decay time of both Ce^{3+} centers might be similar. But that will be investigated in the next round of single bunch measurements with a new apparatus of light detection that will allow the study of the decay process separately for both the Ce^{3+} sites.

An interesting result shown in Fig. 6 is that the intensity did not reduce to the background count (as shown in the inset of Fig. 6) after the pulses and during the ~300 ns time window between excitation pulses. This is an indication that the RL emission also has a slow phosphorescence component, with decay time much longer than 300 ns, when excited with synchrotron radiation, but that component is found to be smaller than ~17% of the peak signal. This part of the signal can be related to the phosphorescence reported by Jia et al. [5] but in that case the authors excited their samples with a mercury bulb lamp and they did not quote how much of the light emission actually decays instantaneously after ceasing the illumination. For practical applications in radiation detection systems that slow the component will not affect the overall time resolution of the scintillator since that is weak enough to be considered as part of the background counts of the detector. Thus, one important conclusion from this work is that the $BaAl_2O_4$:Ce^{3+} is a promising candidate for application in scintillator devices used for fast response.

4. Conclusion

Pure and Ce-doped $BaAl_2O_4$ phosphor was synthesized by proteic sol–gel route. XRD analysis shows that the desired crystalline phase was obtained with a lower temperature than that normally used for conventional solid-state routes. The optical responses, to excitation with monochromatic X-rays, have been studied. The XEOL has been monitored as a function of the X-ray energy around at Ba L_{II-III} edges and Ce L_{III} edge. The XEOL curves increase as the energy of the photons increases. The radioluminescence spectra exhibit two strong broad emissions around 320–480 and 480–650 nm due to the d–f transition. The two strong bands are unfolded due to the presence of Ce^{3+} at two different sites. A decrease of the luminescence when excited at Ce L_{III}-edge is due the energy transfer via X-ray fluorescence, from Ce to Ba in the X-ray photon energy range of the Ce L_{III}-edge absorption. The life time, measured using the single bunch mode synchrotron radiation, revealed that the Ce doped $BaAl_2O_4$ has a fast response with a typical decay time constant of about 44.3 ns. All properties observed in the present work indicate that this material is a candidate for application in fast scintillation devices.

Acknowledgments

The authors are grateful to FINEP, CAPES, INAMI, CNPq and LNLS for financial Support. Research supported by LNLS—Brazilian Synchrotron Light Laboratory/MCT (project XAFS #9358/10).

References

[1] M.J. Weber, Nucl. Instrum. Methods A 527 (2004) 9.
[2] A. Gektin, N. Shiran, S. Neicheva, K. Shimamura, T. Fukuda, Radiat. Prot. Dosim. 100 (2002) 377.
[3] Y. Pei, X. Chen, D. Yao, G. Ren, Radiat. Meas. 42 (2007) 407.
[4] Y. Zorenko, V. Gorbenkoa, I. Konstankevycha, T. Voznjaka, V. Savchyna, M. Niklb, J.A. Maresb, K. Nejezchlebc, V. Mikhailind, V. Kolobanovd, D. Spasskyd, Radiat. Meas. 42 (2007) 528.
[5] D. Jia, X-j. Wang, E. van der Kolka, W.N. Yena, Opt. Commun. 204 (2002) 247.
[6] N. Suriyamurthy, B.S Panigrahi, J. Lumin. 127 (2007) 483.
[7] R. Sakai, T. Katsumata, S. Komuro, T. Morikawa, J. Lumin. 85 (1999) 149.
[8] Z. Qiu, Y. Zhou, M. Lu, A. Zhang, Q. Ma, Acta Mater. 55 (2007) 2615.
[9] Z. Lou, J. Hao, M. Cocivera, J. Phys. D: Appl. Phys. 35 (2002) 2841.
[10] M.A. Macedo, J.M. Sasaki, Processo de Fabricação de Pós Nanoparticulados, INPI 0203876-5.
[11] P.J.R. Montes, M.E.G. Valerio, G.M. Azevedo, Nucl. Instrum. Methods B 266 (2008) 2923.
[12] S.Y. Huang, R. von der Muehll, J. Ravez, J.P. Chaminade, P. Hagenmuller, M. Couzi, J. Solid State Chem. 110 (1994) 97.
[13] D.T. Attwood, Soft X-rays and Extreme Ultaviolett Radiation Principles and Applications, Cambridge University Press, 2000.
[14] P. Dorenbos, J. Alloys Compd. 341 (2002) 156.
[15] J.C. Krupa, M. Queffelec, J. Alloys Compd. 250 (1997) 287.
[16] J.S. Shi, Z.J. Wu, S.H. Zhou, S.Y. Zhang, Chem. Phys. Lett. 380 (2003) 245.

[17] M.V.S. Rezende, M.E.G. Valerio, R.A. Jackson, Opt. Mater. 34 (2011) 109.
[18] M.V.S. Rezende, R.M. Araújo, P.J.R. Montes, M.E.G. Valerio, Opt. Mater. 32 (2010) 1341.
[19] J.A. Mares, A. Beitlerova, M. Nikl, N. Solovieva, C. D'Ambrosio, K. Blazek, P. Maly, K. Nejezchleb, F. Notaristefanid, Radiat. Meas. 38 (2004) 353.
[20] J.A. Mares, M. Nikl, N. Solovieva, C. D'Ambrosio, F. De Notaristefani, K. Blazek, P. Maly, K. Nejezchleb, P. Fabeni, G.P. Pazzi, J.T.M. de Haas, C.W.E. van Eijk, P. Dorenbos, Nucl. Instrum. Methods A 498 (2003) 312.
[21] M. Nikl, E. Mihokova, J.A. Mares, A. Vedda, M. Martini, K. Nejezchleb, K. Blazek, Phys. Status Solidi (a) 181 (2000) R10.
[22] C.M. Combes, P. Dorenbos, C.W.E. van Eijk, J.Y. Gesland, P.A. Rodnyi, J. Lumin. 72 (1997) 753.
[23] C. Dujardin, C. Pedrini, J.C. Gâcon, A.G. Petrosyan, A.N. Belsky, A.N. Vasil'ev, J. Phys.: Condens. Matter 9 (1997) 5229.